Astron. Astrophys. 350, 517–528 (1999)

ASTRONOMY AND ASTROPHYSICS

Time-resolved HST and IUE UV spectroscopy of the intermediate polar FO Aqr⋆

D. de Martino[1], R. Silvotti[1], D.A.H Buckley[2], B.T. Gänsicke[3], M. Mouchet[4], K. Mukai[5,⋆⋆], and S.R. Rosen[6]

[1] Osservatorio Astronomico di Capodimonte, Via Moiariello 16, 80131 Napoli, Italy
[2] South African Astronomical Observatory, P.O. Box 9, Observatory 7935, Cape Town, South Africa
[3] Universitäts Sternwarte Göttingen, Geismarlandstrasse 11, 37083 Göttingen, Germany
[4] DAEC, Observatoire de Paris, Section de Meudon, 92195 Meudon Cedex, France
[5] Laboratory for High Energy Physics, NASA/GSFC, Code 662, Greenbelt, MD 20771, USA
[6] Department of Physics and Astronomy, University of Leicester, University Road, Leicester LE1 7RH, UK

Received 14 June 1999 / Accepted 6 August 1999

Abstract. Time resolved spectroscopy of the Intermediate Polar FO Aqr reveals the presence of multiple periodicities in the UV range. A strong orbital modulation dominates both continuum and emission line flux variabilities, while line velocity motions are only detected at the rotational frequency. A prominent orbital periodicity is also observed in coordinated optical photometry, where FO Aqr was previously found to be spin dominated. The spectral dependence of the main periodicities shows the presence of multi-temperature components in FO Aqr and for the first time a hot and a cool component in the rotational modulation. From a comparison with previous UV and optical data obtained in 1990, no spectral variations in the orbital and rotational variabilities are detected, indicating no significant changes in the effects of X-ray illumination but rather a shrinking of the accretion curtain accompained by an increase in size of the thickened part of the accretion disc. These observations, consistent with the recently discovered long term trend in the X-ray pulsation amplitudes, independently confirm a change in the accretion mode in FO Aqr, which switched from a disc-fed into a disc-overflow state, likely triggered by mass accretion variations.

Key words: accretion, accretion disks – stars: binaries: close – stars: individual: FO Aqr – ultraviolet: stars – X-rays: stars

1. Introduction

Intermediate Polars (IPs) are a subclass of magnetic Cataclysmic Variables which consist of an asynchronously rotating ($\mathrm{P_{spin}} < \mathrm{P_{orb}}$) magnetized white dwarf accreting from a late type, main sequence, Roche-lobe filling secondary star (Patterson 1994; Warner 1995).

Send offprint requests to: D. de Martino (demartin@na.astro.it)

⋆ Based on observations collected with the NASA/ESA Hubble Space Telescope, obtained at the Space Telescope Science Institute and with the International Ultraviolet Explorer, obtained from the IUE Final Archive at VILSPA

⋆⋆ Universities Space Research Association

Except for a few systems for which polarized optical/IR emission is detected, the white dwarf is believed to possess a weak ($\lesssim 2$ MG) magnetic field which dominates the accretion flow only at a few radii from its surface. Within the magnetospheric radius, material is channeled towards the magnetic polar regions in an arc-shaped accretion curtain (Rosen et al. 1988). At larger distances, different accretion patterns can be present: a truncated accretion disc (disc-fed systems), direct accretion from the stream onto the magnetosphere (disc-less systems) as well as a combination of the two, where the stream material overpasses the disc (disc-overflow) (Hellier 1995 and references therein).

Due to the asynchronous rotation, IPs show a wide range of periodicities at the white dwarf spin (ω), the orbital (Ω) and sideband frequencies (Warner 1986; Patterson 1994, Warner 1995), whose amplitudes can be different in different spectral ranges (de Martino 1993). FO Aqr (H2215-086) was known to show strong periodic X-ray, optical and IR pulsations at the spin frequency, $\omega = 1/(\mathrm{P_{spin}} = 20.9\,\mathrm{min})$, and lower amplitude variations at the orbital $\Omega = 1/(\mathrm{P_{orb}} = 4.85\,\mathrm{hr})$ and beat $\omega - \Omega = 1/(\mathrm{P_{beat}} = 22.5\,\mathrm{min})$ frequencies (de Martino et al. 1994, hereafter Paper 1, and references therein; Marsh & Duck 1996; Patterson et al. 1998). The dominance of the spin pulsation at optical and high X-ray energies (>5 keV) can be accounted for by a disc-fed accretion, whose evidence was provided by a partial eclipse in the optical continuum and emission lines (Hellier et al. 1989; Mukai et al. 1994; Hellier 1995). FO Aqr was also found to possess a disc-overflow accretion mode (Hellier 1993), and the recent evidence of a long term variability in the amplitudes of the X-ray pulsations has been interpreted as changes in the accretion mode (Beardmore et al. 1998). This kind of variability, only recently recognized, is also observed in other IPs like TX Col (Buckley 1996; Norton et al. 1997) and BG CMi (de Martino et al. 1995).

The identification of the actual accretion geometry and the determination of energy budgets of the primary X-ray and secondary reprocessed UV, optical and IR emissions reside on multi-wavelength observations. The main modulations in

Table 1. Journal of observations.

Instrument	Date	UT_{start} hh:mm:ss	Duration s
HST/FOS			
Slot 1	1995 Sept. 10	14:11:04	2332
Slot 2	1995 Sept. 10	15:45:11	2461
Slot 3	1995 Sept. 10	17:21:18	2461
Slot 4	1995 Sept. 10	18:57:49	2461
Slot 5	1995 Sept. 10	20:34:22	2461
Slot 6	1995 Sept. 10	22:10:54	2461
IUE Image #			
SWP56089	1995 Oct. 15	14:44:13	2520
SWP56090	1995 Oct. 15	16:21:26	2520
SWP56091	1995 Oct. 15	18:01:17	2520
SWP56092	1995 Oct. 15	19:22:39	2520
SWP56093	1995 Oct. 15	20:38:56	2520
SWP56094	1995 Oct. 15	22:02:27	2520
SWP56095	1995 Oct. 15	23:29:51	2520
SWP56096	1995 Oct. 16	00:57:16	2520
SWP56097	1995 Oct. 16	02:24:39	2520
SWP56098	1995 Oct. 16	03:55:35	2520
LWP31592	1995 Oct. 15	13:45:09	2520
LWP31593	1995 Oct. 15	15:34:55	2520
LWP31594	1995 Oct. 15	17:17:11	2520
LWP31595	1995 Oct. 15	18:45:29	1260
LWP31596	1995 Oct. 15	20:06:28	1260
LWP31597	1995 Oct. 15	21:25:29	1260
LWP31598	1995 Oct. 15	22:46:08	2520
LWP31599	1995 Oct. 16	00:13:32	2520
LWP31600	1995 Oct. 16	01:41:01	2520
LWP31601	1995 Oct. 16	03:26:04	1260
SAAO			
BVRI	1995 Oct. 18	18:37:44	13758
	1995 Oct. 19	19:41:11	2745
	1995 Oct. 20	20:01:30	7480
No Filter	1995 Oct. 21	18:04:35	15585
	1995 Oct. 23	18:40:20	9130

FO Aqr have been studied in the X-rays and at optical/IR wavelengths. The optical spin pulsations, occurring mostly in phase with the X-ray ones, were found to arise from the outer regions of the accretion curtain (Paper 1; Welsh & Martell 1996). The orbital modulation from UV to IR was instead found to be multicomponent and attributed to the X-ray heated azimuthal structure of the accretion disc (henceforth bulge) and to the inner illuminated face of the secondary star (Paper 1). However the temperature of the UV emitting bulge could not be constrained due to the lack of a precise quantification of the spectral shape of the UV spin modulation. In this work we present high temporal resolution spectroscopy acquired with HST/FOS which provides the first detection of different UV periodicities in FO Aqr. For a comprehensive study, these data are complemented with low temporal resolution IUE spectra along the orbital period. Coordinated optical photometry extends the study to a wider spectral range, providing the link to investigate the long term behaviour of these variabilities.

2. Observations and data reduction

The UV and optical campaign on FO Aqr was carried out between September and October 1995 with HST, IUE and at the South African Astronomical Observatory. The journal of the observations is reported in Table 1.

2.1. The HST data

HST Faint Object Spectrograph observations of FO Aqr were performed on September 10, 1995. The observations were carried out in the rapid mode during 7 consecutive HST orbits. Due to target acquisition procedures the total effective on source exposure time was 4.07 h, yielding six continuous exposure slots as detailed in Table 1. The orbital period was unevenly sampled since it is commensurable with the HST orbit. The G160L grating was operated with the blue digicon covering the range 1154–2508 Å at a resolution of 6.8 Å diode^{-1} and with the 0.86″ upper square aperture, supposed to be free from the 1500–1560 Å photocathode blemish which is known to affect the circular apertures (HST Data Handbook, 1997). A total of 797 spectra were collected, each with an effective exposure time of $\sim$ 18 s.

The standard routine processing ST ScI pipeline applied to the data at the time of the observations revealed the presence of anomalous features when comparing the reduced spectra with the IUE data, and in particular in the regions 1500–1590 Å and 1950–2010 Å . The data were then re-processed using the STSDAS/CALFOS routine within IRAF using the latest reference files for sensitivity correction and appropriate aperture flatfield provided by the ST ScI Spectrograph Group in summer 1998. The calibrated spectra appear then free from the above features although the IUE fluxes are on average $\sim$ 1.1 times larger than the FOS ones (see Fig. 1). A check against systematic effects using spectra of standard stars observed with both IUE and FOS only confirms the known lower flux (on average of $\sim 7\%$) of IUE, with respect to that of FOS (Gonzalez-Riestra 1998). The residual flux difference may be due to the fact that the IUE data were acquired a month later than the FOS spectra.

The G160L grating provides zero order light covering the full range between 1150 and 5500 Å, with an effective wavelength at 3400 Å, which provides useful simultaneous broadband photometry. The flux calibration of the zero-order signal (Eracleous & Horne 1994) updated for errors and post-COSTAR sensitivity and aperture throughput (HST Data Handbook 1997) has been applied to the signal extracted in the zero-order feature of each of the 797 exposures.

2.2. The IUE data

On October 15, 1995 ten IUE SWP (1150–1980 Å) and ten LWP (1950–3200 Å) low resolution ($\sim$ 6 Å) spectra were acquired during consecutive 16 h with exposure times equal or twice the

P_{spin} to smear out effects of the rotational pulsation (Table 1). The SWP and LWP exposures sample the orbital period.

The spectra have been re-processed at VILSPA using the IUE NEWSIPS pipeline used for the IUE Final Archive which applies the SWET extraction method as well as the latest flux calibrations and close-out camera sensitivity corrections (Garhart et al. 1997). Line-by-line images have been inspected for spurious features which have been identified and removed.

2.3. The optical photometry

Optical photometry was conducted in the period October 18–23 1995 at the SAAO 0.75 m telescope and UCT Photometer employing a Hamamatsu R93402 GaAs photomultiplier. BVRI (Cousins) photometry was carried out on the first three nights performing symmetric modules with integration times of 30 s or 20 s respectively for the B and I, or V and R filters. The typical time resolution for the sequence of all four filters was ∼120 s, with interruption every ∼ 10 min for sky measurements. The times and durations of individual runs are reported in Table 1. The orbital period has not been fully sampled.

Additional fast photometry in white light has been carried out on October 21 and 23, 1995 using the same photometer, but employing a second channel photomultiplier for monitoring of a nearby comparison star. Continuous 5 s integrations were obtained, with occasional interruptions (every 15–20 min) for sky measurements (lasting ∼ 20–30 s). During the two nights, the observations were carried out for 4.3 h and 2.5 h respectively.

The photometric data have been reduced in a standard manner with sky subtraction, extinction correction and transformation to the standard Cousins system using observations of E-region standards obtained on the same night.

3. The UV spectrum of FO Aqr

The grand average UV spectra of FO Aqr as observed with FOS and IUE are shown in Fig. 1 (upper panel), where the above flux difference is apparent.

The UV luminosity in the 1150–3200 Å IUE range is $6 \times 10^{32}\,\mathrm{ergs\,s^{-1}}$assuming a distance of 325 pc (Paper 1), a factor 1.3 larger than during previous UV observations in 1990. The optical photometry also indicates a brightening of 0.17 mag between the two epochs, indicating long term luminosity variations (see also Sect. 8.5)

The UV spectrum of FO Aqr is typical of magnetic CVs (Chiappetti et al., 1989; de Martino 1995) with strong emissions of N V $\lambda1240$, Si IV $\lambda1397$, C IV $\lambda1550$, He II $\lambda\lambda1640, 2733$ and Mg II $\lambda2800$. The weaker Si IV with respect to N V emission, classes the IP nature (de Martino 1995). Weaker emissions from lower ionization states of different species such as C III $\lambda1176$, the blend of Si III $\lambda1298$ multiplet, Si II $\lambda1304$ and geocoronal O I $\lambda1305$, Si III $\lambda1895$, Si II $\lambda1808$, N IV $\lambda1718$, N III $\lambda1747 - 1754$, Al III $\lambda1855$ and Al II $\lambda1670$, as well as He II $\lambda2307$, possibly blended with C III $\lambda2297$, and He II $\lambda2386$, are identified in the higher quality FOS spectrum. Also weak oxygen lines of O IV $\lambda1343$ and O V $\lambda1371$ are detected.

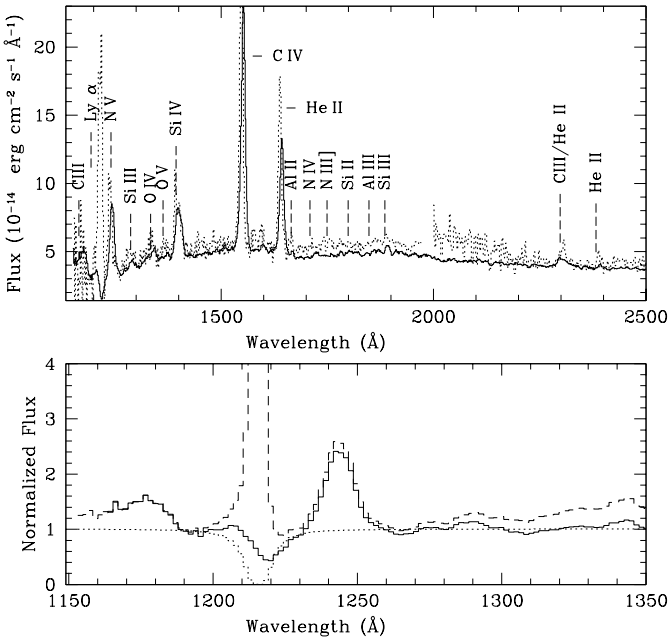

Fig. 1. *Upper panel:* Grand average FOS (solid line) and IUE (dotted line) spectra of FO Aqr in the range 1150–2500 Å together with line identification. *Bottom panel:* Enlargement of the Lyα feature in the average FOS spectrum. The solid line represents the observed spectrum, the dotted line a damped Lorentzian profile convolved with a 7 Å FWHM gaussian corresponding to $N_{\rm H} = 5 \times 10^{20}\,\mathrm{cm^{-2}}$ and the dashed line represents the ratio between the two, enhancing the emission feature at 1215 Å .

Some of these lines are also observed in the HST/FOS spectra of AE Aqr (Eracleous & Horne 1994), DQ Her (Silber et al. 1996) and PQ Gem (Stavroyiannopoulos et al. 1997). The presence of high ionization species together with extremely weak emissions (E.W. < 1 Å) of lower ionization species are characteristic of a higher ionization efficiency in IPs with respect to Polars (de Martino 1998). The line ratios N V/Si IV and N V/He II, when compared with photoionization models developed by Mauche et al. (1997) are close to the predicted values for an ionizing blackbody spectrum at 30 eV.

In contrast to the IUE spectra, the FOS data allow us to finally detect the intrinsic Lyα $\lambda1216$ line. This appears to be composed of a relatively deep (E.W.=5.4±0.1 Å) absorption and a weak emission (E.W.=1.4±0.1 Å). The center wavelength of the absorption feature is however red-shifted by ∼4 Å with respect to rest wavelength and other emission line positions, while the weak emission is blue-shifted at 1206 Å in the grand average spectrum. Discussion on the nature of this feature is left until Sects. 5 and 7, however the Lyα absorption provides an upper limit to the hydrogen column density along the line of sight to FO Aqr.

A pure damping Lorentzian profile (Bohlin 1975) convolved with a 7 Å FWHM Gaussian has then been fitted to the Lyα absorption line (Fig. 1, bottom panel). The resulting neutral hydrogen column density is $N_{\rm H} = (5.0 \pm 1.5) \times 10^{20}\,\mathrm{cm^{-2}}$. The residual from the fit shows an emission line with maximum flux

at ~ 1215 Å , probably geocoronal or intrinsic, with an excess of flux in the blue wing possibly due to emission of Si III λ1206.

The derived value for $N_{\rm H}$ is consistent with the total interstellar column density in the direction of FO Aqr as derived from Dickey & Lockman (1990) and with the upper limit estimated from X-rays (Mukai et al. 1994). Assuming an average gas-to-dust ratio (Shull & van Steenberg 1985), this upper limit corresponds to a reddening of $\rm E_{B-V} \approx 0.1$. Although FO Aqr was already known to be negligibly reddened from IUE observations (Chiappetti et al. 1989), an upper limit $\rm E_{B-V} = 0.013\pm$ 0.005 is derived from the absence of the 2200 Å absorption in the FOS data. This indicates that, despite the coincidence, most of the neutral absorption is unrelated to the interstellar dust and hence it is likely located within the binary system.

4. Time series analysis

The presence of periodicities in FO Aqr has been investigated in the FOS continua, emission lines and zero-order light as well as in the optical photometric data.

4.1. HST UV data

Fluxes in five line-free continuum bands have been measured in each FOS spectrum in the ranges λ1265–1275, λ1425–1450, λ1675–1710, λ2020–2100, λ2410–2500. Line fluxes of He II λ1640, N V, Si IV and C IV and $\rm Ly\alpha$ have been computed adopting a method which uses for the continuum a power law distribution as found from a fit in the above continuum bands. Furthermore, since the low spectral resolution of FOS data prevents the study of UV line profiles, measures of the V/R ratios of emission lines have been used to investigate possible motions in the lines. These are defined as the ratios between the integrated fluxes in the violet and red portions of the emission lines assuming as centroid wavelength that measured in the average profile. Such analysis is restricted to the strong emissions of He II, C IV and N V lines whose FWZI are $\pm 3000\,\rm km\,s^{-1}$, $\pm 4000\,\rm km\,s^{-1}$and $\pm 3000\,\rm km\,s^{-1}$ respectively.

In order to detect the active frequencies in the power spectrum and to optimize the S/N ratio, a Fourier analysis has been performed using the DFT algorithm of Deeming (1975) on the total UV continuum (sum of the five bands) and line (sum of N V, Si IV, C IV and He II) fluxes and zero-order light. From Fig. 2, the dominance of the Ω variability is apparent, being about twice the ω signal, as well as the presence of substantial power at the sideband and orbital harmonic frequencies. To distinguish real signals from artifacts due to the sampling of the HST orbit, a least-square technique was applied to the each data set which fits simultaneously multiple sinusoids at fixed frequencies. A synthetic light curve with the same temporal sampling of the data was created and subtracted (residuals). The continuum and zero-order light reveal, besides the ω and Ω frequencies, also the $\omega - 2\,\Omega$, $\omega - \Omega$ and $\Omega + \omega$ sidebands, whereas in the emission lines the $2\,\Omega$ and $\omega - \Omega$ frequencies are detected. In Fig. 2 the amplitude spectra relative to the multiple sinusoids and the residuals are also shown for comparison. It should be noted that peaks at $\sim 54\,\rm day^{-1}$ and $\sim 84\,\rm day^{-1}$ are identified as sideband fequencies of the spin and HST orbital frequencies. These are removed by the method as shown by the residuals. Then a five (four) frequency composite sinusoidal function for each spectral band (emission line) has been used and the derived amplitudes, reported in Table 2, have been compared with the average power in the DFTs of the residuals (σ) in the range of frequencies of interest (i.e. $\nu \lesssim 1.4$ mHz), (Column 8). While the signals at $\omega - 2\,\Omega$ (continuum) and at 2Ω (emission lines) on average fulfil a 4 σ criterium, the other sidebands are between between 2.1 and 3.5 σ.

A further check has been performed using the CLEAN algorithm (Roberts et al. 1987) which removes the windowing effects of the HST orbit. The CLEANED power spectra, adopting a gain of 0.1 and 500 iterations, indeed reveal the presence of the $\omega - 2\Omega$ and $\omega - \Omega$ sidebands in the continuum and the 2Ω in the emission lines. The lack of significant power at the other frequencies is consistent with the previous analysis. Hence, these weakly active frequencies will be considered with some caution in this analysis.

A strong colour effect in the UV continuum is detected with amplitudes decreasing at longer wavelengths. Different from other lines is the behaviour in the $\rm Ly\alpha$ feature, whose absorption component is modulated at the Ω frequency, while a variability at the spin is at a 2σ level. No significant variations are detected in the equivalent width of the absorption as well as in the emission component.

In contrast to the flux behaviour, the V/R ratios are variable only at the ω frequency (Fig. 2, bottom panels). Noteworthy is the marginal spin variability in the C IV line. The amplitudes of the spin modulation, obtained from the least-square fits, are reported in the last column of Table 2.

4.2. Optical data

The analysis of BVRI data acquired during three nights has been performed following the same procedure adopted for the HST data. Contrary to previous observations, the orbital variability also dominates in the optical being ~ 1.5 times the spin modulation. The presence of sideband modulations is more uncertain because of the lower quality of the data. Nevertheless, to ensure uniformity between UV and optical results, a least-square fit to the data has been applied using the same five frequency sinusoidal function, i.e. Ω, ω, $\omega - 2\,\Omega$, $\omega - \Omega$, $\omega + \Omega$. The resulting amplitudes, reported in Table 2, when compared with the noise in the residuals (Column 8), can be considered as upper limits.

As far as the fast photometry is concerned, the low quality of the data only allows the detection of the spin and orbital variabilities. In particular, the latter is detected on the first night with a pronounced dip which is not consistent with the refined orbital ephemeris based on orbital minima recently given by Patterson et al. (1998), which defines the inferior conjunction of the secondary star. Therefore these data will not be used for a multi-wavelength analysis of the pulsations.

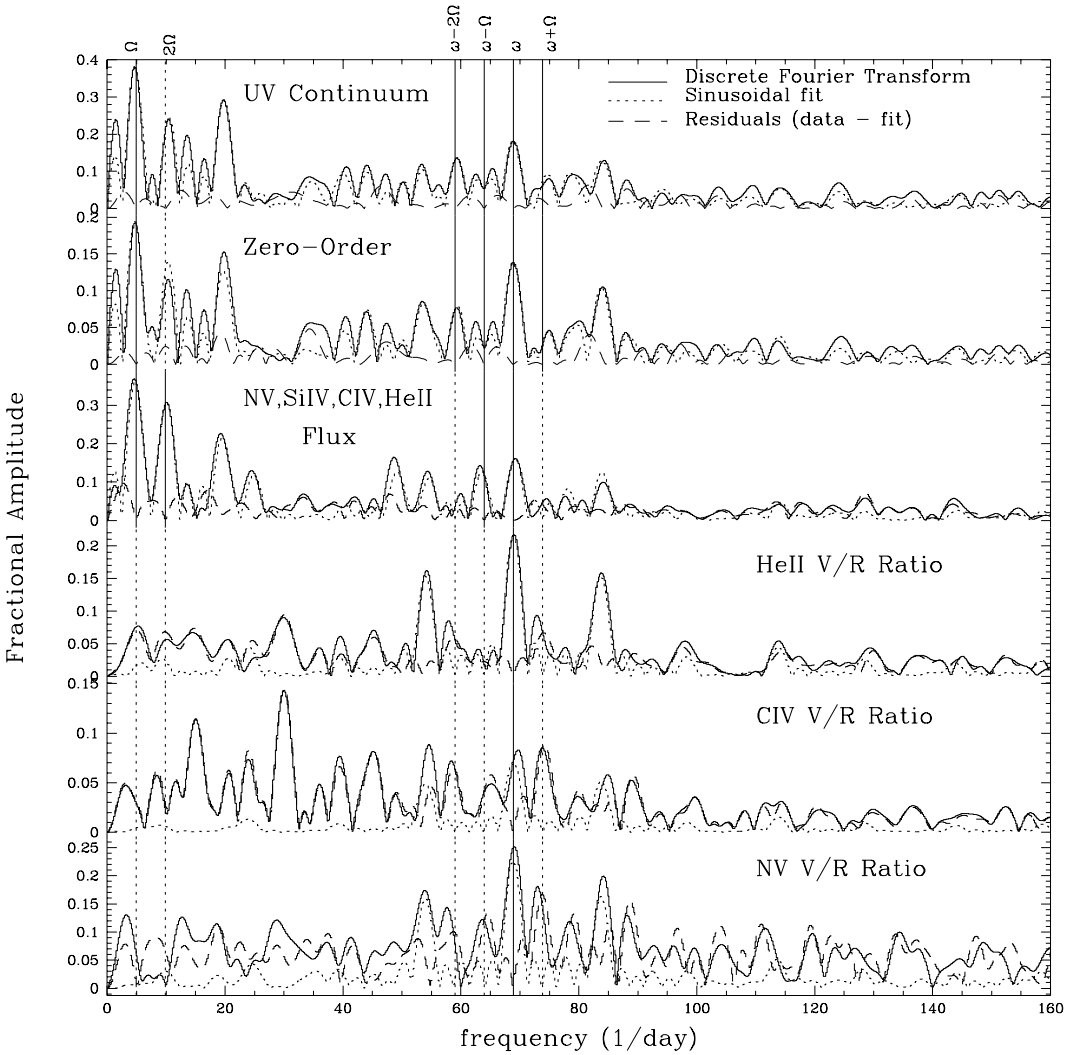

Fig. 2. From top to bottom: DFTs of the UV continuum, zero-order light, emission line fluxes and V/R ratios of He II, C II and N V (solid line). DFTs of the sinusoidal functions (dotted line) together with those of the residuals (dashed line) are also shown. The frequencies used in the multiple sinusoidal fits are marked with vertical solid lines.

From this analysis new times of maxima for the orbital and rotational modulations are derived for the UV continuum and optical light:

$HJD^{\rm max}_{\rm orb} = 2\,449\,971.2251 \pm 0.0006$ in the UV;
$HJD^{\rm max}_{\rm spin} = 2\,449\,971.11181 \pm 0.00010$ in the UV;
$HJD^{\rm max}_{\rm orb} = 2\,449\,971.2235 \pm 0.0034$ in the optical;
$HJD^{\rm max}_{\rm spin} = 2\,449\,971.11021 \pm 0.00035$ in the optical;

Both UV and optical orbital maxima lead by $\Delta\Phi_{\rm orb}$ = 0.145 those predicted by Patterson et al.'s ephemeris. Such phase difference, discussed in Sect. 7, is consistent with the previous UV results (Paper 1).

On the other hand, the optical rotational maximum agrees within 8 per cent with that predicted by the new revised cubic ephemeris given by Patterson (1998, private communication):

$$HJD\,2\,444\,782.9168(2) + 0.014519035(2)\,E + 7.002(7)\,10^{-13}\,E^2 - 1.556(2)\,10^{-18}\,E^3 \quad (1)$$

The UV rotational pulses lag the optical by $\Delta\Phi_{\rm rot} = 0.186$. Such colour effect will be discussed in more detail in Sect. 5.

Furthermore, the time of coherence between spin and beat modulations is found to be $HJD_{\rm co}$ = 2 449 971.2335 ± 0.0070 in both UV and optical. Throughout this paper the Patterson et al.'s orbital ephemeris will be used but $\Phi_{\rm orb}$ = 0.0 will refer to the orbital maximum. Hence, phase coherence occurs at $\Phi_{\rm orb} = 0.90 \pm 0.03$. i.e. close to the orbital maximum, whilst in 1988 and 1990 it was found close to the orbital minimum (Osborne & Mukai 1989; Paper 1). Such phase changes are not uncommon for FO Aqr (Semeniuk & Kaluzny 1988; Hellier et al. 1990).

5. The rotational modulation

UV continuum, zero-order light, and UV emission line fluxes as well as their V/R ratios have been folded in 56 phase bins along $P_{\rm spin}$. The spin pulses, pre-whitened from all other frequency variations, are shown in Fig. 3 together with the optical B band

Table 2. Amplitudes of the modulations for the UV continuum, optical and UV emission lines derived from a multicomponent sinusoidal fit.

Band (Å)	A_Ω	$A_{2\Omega}$	A_ω	$A_{\omega-2\Omega}$	$A_{\omega-\Omega}$	$A_{\omega+\Omega}$	$\bar{A}_{res}$	$A_\omega(V/R)$
1265 – 1275	1.730(52)		0.893(51)	0.913(72)	0.391(55)	0.693(72)	0.181	
1425 – 1450	1.784(42)		0.867(43)	0.694(59)	0.453(44)	0.441(61)	0.166	
1675 – 1710	1.779(37)		0.738(37)	0.685(51)	0.344(37)	0.420(52)	0.157	
2020 – 2100	1.416(29)		0.656(29)	0.553(40)	0.303(30)	0.334(41)	0.125	
2410 – 2500	1.130(25)		0.627(25)	0.463(34)	0.236(25)	0.257(34)	0.108	
2900 – 2985	0.942(45)							
Zero-Order	0.578(15)		0.417(14)	0.323(21)	0.120(15)	0.178(21)	0.062	
B	0.354(25)		0.259(38)	0.025(33)	0.046(35)	0.047(31)	0.045	
V	0.182(14)		0.129(22)	0.050(19)	0.006(21)	0.023(18)	0.026	
$\mathbf{R}_c$	0.134(13)		0.091(20)	0.026(16)	0.020(21)	0.037(16)	0.021	
$\mathbf{I}_c$	0.109(10)		0.054(16)	0.022(14)	0.031(17)	0.015(13)	0.016	
N V flux	14.37(1.98)	6.75(1.97)	12.75(1.37)		12.25(1.37)		3.32	0.256(41)
Si IV flux	15.40(1.54)	13.17(1.53)	7.60(1.07)		7.77(1.07)		2.75	
C IV flux	77.10(2.87)	36.74(2.86)	35.71(1.98)		22.22(1.99)		16.99	0.057(08)
He II flux	31.81(1.59)	14.68(1.60)	22.57(1.10)		13.40(1.11)		2.75	0.173(10)
Lyα abs.	23.35(1.08)		6.83(1.07)				3.41	

Notes: (1) Continuum flux amplitudes are in units of $10^{-14}\,\mathrm{ergs\ cm^{-2}s^{-1}\AA^{-1}}$ while line fluxes are in units of $10^{-14}\,\mathrm{ergs\ cm^{-2}s^{-1}}$. Errors in parentheses are referred to the last significant digits.
(2) $\bar{A}_{res}$ is the average amplitude of the DFT of the residuals, calculated for frequencies $\lesssim$1.4 mHz.
(3) For the $\lambda\lambda$ 2900–2985 band only the orbital amplitude is reported as derived from IUE data.

pulses folded in 28 phase bins. A strong colour effect is observed in both amplitudes and phasing. Fractional amplitudes (amplitudes of the sinusoid $\mathrm{Asin}(\omega \mathrm{t}+\phi)$ divided by the average value) decrease from 26% in the far-UV to 16% in the near-UV and to 10% in the optical. The far-UV pulse maximum is broader and lags by $\Delta\phi_{\rm spin} = 0.091 \pm 0.010$ and 0.186±0.008 the near-UV and optical maxima respectively. While the UV line fluxes follow the near-UV modulation, their V/R ratios are in phase with the far-UV, with a maximum blue shift when the far-UV pulse is at maximum. The pulsation in the line fluxes are 18%, 12%, and 10% in He II, C IV and Si IV. The V/R ratios are generally <1 indicating the presence of a dominant blue component in the lines, which is also visible from the extended blue wings in the average spectrum. The velocity displacements indicate the presence of a spin S-wave in the line profiles similar to the optical (Hellier et al. 1990). Both continuum and emission lines therefore strongly indicate the presence of two components which affect the rotational modulation in FO Aqr.

The 797 FOS spectra have been spin-folded into 20 phase bins. A total of 780 light curves, each sampling a wavelength bin of ~ 1.8 Å , were then produced and fitted with a sinusoid. The resulting amplitudes define the rotational pulsed spectrum as $\mathrm{F}_\lambda = 2\,\mathrm{A}_\lambda$. This spectrum (shown in the enlargement of the lower panel of Fig. 3), has to be regarded as an upper limit to the modulated flux since no pre–whitening could be performed given the low S/N of each 780 light curves. This spectrum gives evidence of modulation not only in the main emission lines and Lyα absorption but also in the weaker emission features identified in Sect. 3. Broad band UV continuum and optical photometric spin pulsed fluxes, obtained from the multi-frequency fit and reported in Fig. 3, provide a correct description of the rotational pulsed energy distribution. A spectral fit to the broad band UV and optical spectrum, using a composite spectral function, consisting of two blackbodies, gives 37 500±500 K and 12 000±400 K ($\chi^2_{\rm red} = 0.91$). The projected fractional area of the hot component is $\sim$0.11 $\mathrm{A_{wd}}$, while the cool one covers $\sim 10.7\,\mathrm{A_{wd}}$, for $\mathrm{R_{wd}} = 8 \times 10^8$ cm, and d=325 pc (Paper 1).

The FOS rotational pulsed spectrum shows the presence of a Lyα absorption feature which gives a hydrogen column density of $8 \pm 2 \times 10^{20}\,\mathrm{cm^{-2}}$. On the other hand, assuming $N_{\rm H} = 5 \times 10^{20}\,\mathrm{cm^{-2}}$, as derived from the grand average spectrum, a composite function consisting of a white dwarf model atmosphere with at 36 000 K and of the same 12 000 K blackbody gives an equally satisfactory fit to the whole FOS spectrum. For a distance of 325 pc the radius of the white dwarf is 4.9×10^8 cm, in agreement with that of the hot blackbody component.

While the detection of the hot component is new, a comparison with previous spectral analysis of the optical and IR spin pulses observed in 1990 shows that the temperature of the cool component has not changed with time but instead it suffered a decrease in area by a factor of ~ 1.5.

6. The sideband modulations

The beat $\omega - \Omega$ modulation, although weak among the detected sidebands, shows an anti-phased behaviour between line fluxes and continuum (Fig. 4a). The UV line fluxes, with average fractional amplitudes of $\sim 11\%$, show a minimum when the UV continuum is maximum. Their maximum shows a dip-like feature centered on the UV continumm minimum. Colour effects are also encountered, the far-UV pulses being stronger ($\sim 11\%$) than the near-UV ($\sim 6\%$) ones and lagging by ~ 0.2 in phase the

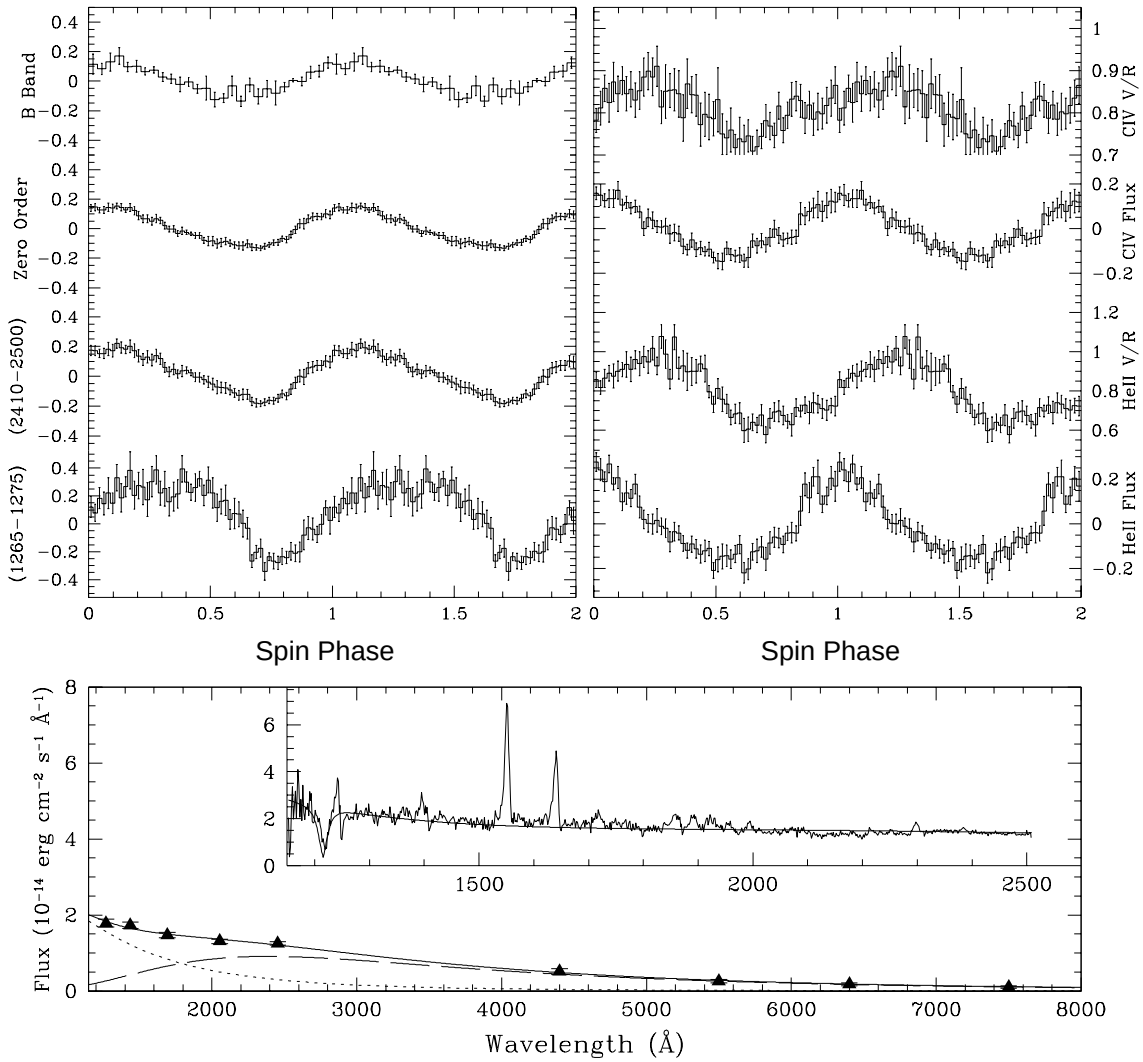

Fig. 3. *Upper left:* Spin pulses in the far-UV, near-UV, zero order and B band (upper left panel). *Upper right:* C IV and He II flux and V/R rotational curves. Fluxes are fractional as described in the text, the average value has been subtracted. *Bottom panel:* Rotational broad band UV and optical energy distribution together with the best fit composite function: a hot (37 500 K) (dotted line) and a cool (12 000 K) (long-dashed line) blackbody function (sum: solid line). A composite function (solid line) consisting of a 36 000 K white dwarf model spectrum and of the same 12 000 K blackbody absorbed by $N_{\rm H} = 5 \times 10^{20}\,{\rm cm}^{-2}$ is shown in the insert figure together with the FOS rotational pulsed spectrum described in the text.

near-UV. The trend of a decrease in the amplitudes at increasing wavelengths is confirmed in the optical where an upper limit of $\sim 2\%$ can be set to the fractional amplitudes.

A similar colour effect is also observed in the $\omega+\Omega$ sideband pulsation with fractional amplitudes ranging from $\sim 20\%$ in the far-UV to $\sim 7\%$ in the near-UV, displaying a broadening of the maximum towards longer wavelengths (Fig. 4b).

The strong $\omega - 2\,\Omega$ pulsation only shows a wavelength dependence in the fractional amplitudes, being in the far-UV $\sim 26\%$ and decreasing to $\sim 12\%$ in the near-UV (Fig. 4c) and to $\sim$ 2–3% (upper limit) in the optical.

The modulated spectra at the three frequencies have been derived following the same procedure as for the rotational pulsed spectrum. The anti-phased behaviour of the emission lines is seen in the beat pulsed spectrum, where these are seen as absorption features, except for residuals in the C IV and He II lines (Fig 4d, bottom panel). The modulation spectra at $\omega - 2\Omega$ and $\omega + \Omega$ frequencies show weak emissions at Si IV, C IV and He II indicating a marginal variability at these frequencies. The UV continuum energy distributions of these variabilities are best represented by power laws $F_\lambda \propto \lambda^{-\alpha}$ with spectral index $\alpha \sim 0.8$–1.7, rather than blackbodies (20 000–25 000 K), possibly suggesting that more than one component is acting. Given the low level of confidence of the sideband variabilities it is not possible to derive further information.

7. The orbital variability

The UV and optical orbital modulations have been investigated folding the FOS continuum broad band and emission line fluxes in 28 orbital phase bins. The light curves have been prewhitened

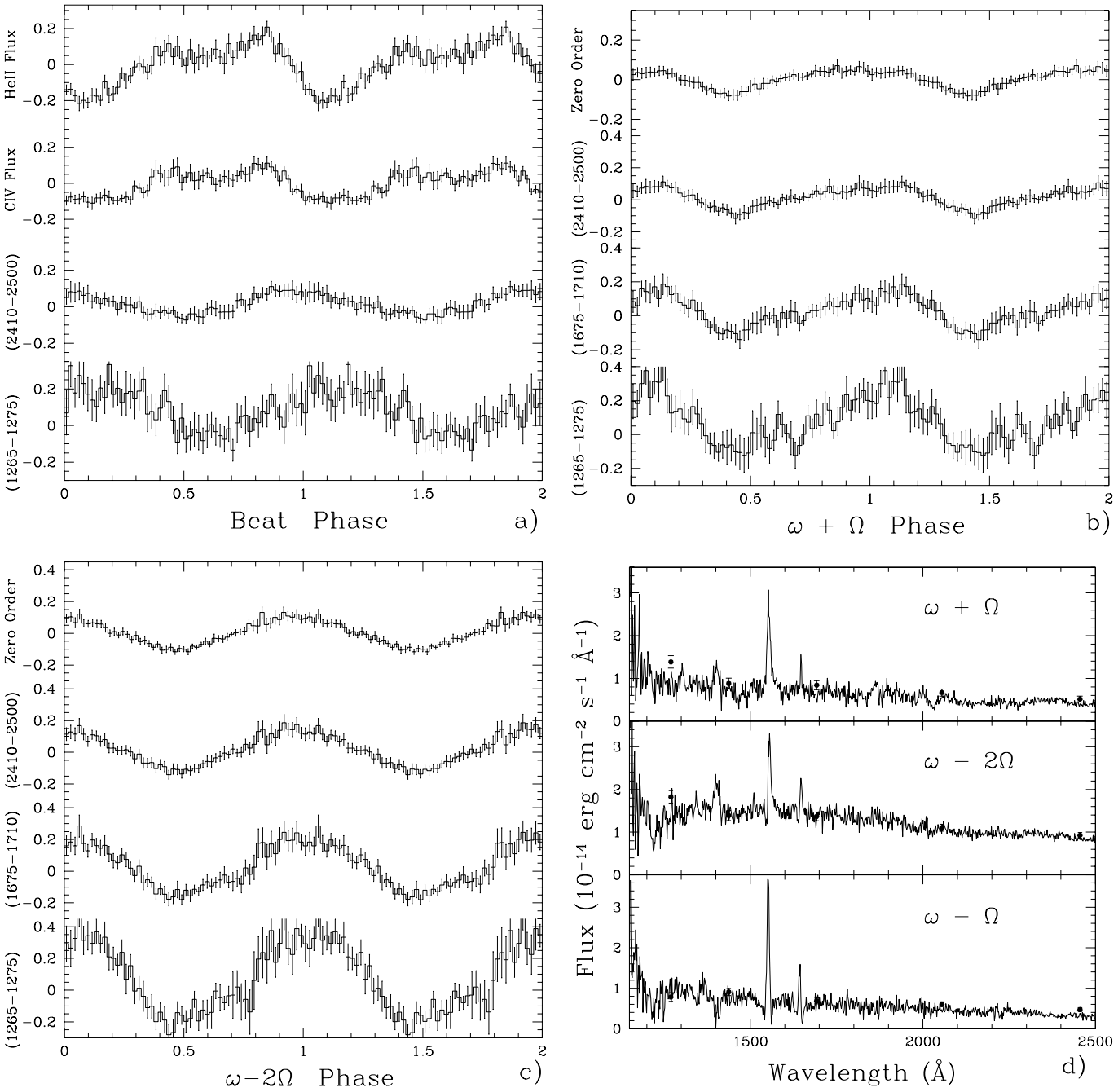

Fig. 4. a The beat $\omega - \Omega$ modulation in the far-UV, near-UV continua and line fluxes of C IV and He II. **b** The $\omega + \Omega$ and **c** the $\omega - 2\,\Omega$ light curves in three UV bands and zero order light. Fluxes are fractional. **d** From bottom to top, the pulsation spectra at the beat $\omega - \Omega$, $\omega - 2\,\Omega$ and $\omega + \Omega$ frequencies (solid line) together with broad band UV fluxes derived from the multi-frequency fits (filled circles).

by the other active frequencies using the results of the multi-frequency fits. For the IUE data, continuum broad band and emission line flux measures have been performed on each SWP and LWP spectrum. Three broad bands have been selected in each spectral range, five of them coinciding with the FOS selected bands and a sixth one in the range λ 2900–2985. The contribution of the spin pulsation, as derived from the multi-frequency fit has been removed. The best fit blackbody spin pulsed spectrum has been used to allow prewhitening in the range λ2900–2985. The FOS and IUE broad band continuum fluxes in the far-UV, mid-UV and near-UV as well as the zero order and B band light curves are reported in the left panel of Fig. 5, while the emission line fluxes of Si IV, C IV and He II are shown in the right panel. The orbital gaps due to the HST sampling are apparent.

A strong colour dependence is encountered in the modulation amplitudes as well as the phasing. Fractional amplitudes range from 40% in the far-UV to 28% in the near-UV (IUE

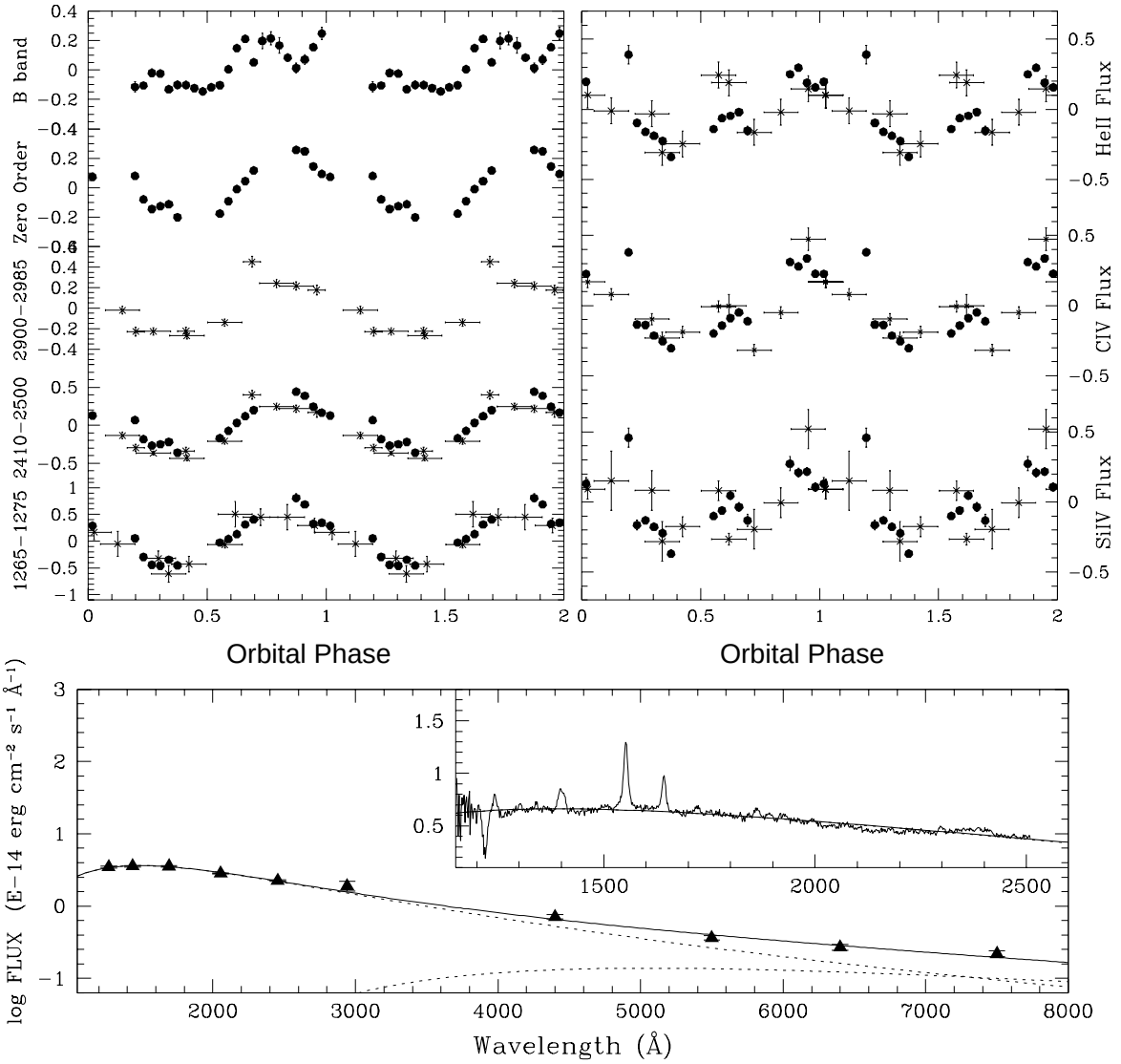

Fig. 5. *Upper left:* Orbital modulation in the far-UV, mid-UV and near-UV, zero order and B light (upper left panel). *Upper right:* Si IV, C IV and He II flux light curves. Fluxes are fractional as described in the text and the average value has been subtracted. The IUE measures are reported together with their phase coverage. *Bottom panel:* The orbital broad band UV and optical modulated fluxes represented with the best fit (solid line) composite function as described in the text. The two blackbodies are represented with dotted lines. A hot (21500 K) blackbody function describes the UV FOS spectrum (shown in the inserted figure.)

band) and 15% in the optical. The modulation amplitudes then have increased by a factor ~ 2.5 in the UV and ~ 1.5 in the optical with respect to 1990. However, the phasing of UV maximum and minimum has not changed with time, occurring at $\Phi_{\rm orb} = 0.86$ and $\Phi_{\rm orb} = 0.34$, respectively. The UV modulation is more sinusoidal, whilst the optical light curve is more structured with a double humped maximum between $\Phi_{\rm orb}$ = 0.75 and $\Phi_{\rm orb}$ = 0.0. A comparison with the optical behaviour in 1990 indicates an absence of a broad maximum centered at $\Phi_{\rm orb}$ = 0.0 and a less defined minimum. The current observations are inadequate to resolve the orbital dip due to a grazing eclipse of the accretion disc in either UV and optical ranges.

The orbital modulation in the UV emission line fluxes is strong with fractional amplitudes of 40% in N V, 20% in Si IV, 29% in C IV and 23% in He II and almost in phase with the UV continuum.

The spectrum of the UV orbital variability derived with the same procedure as described before is shown in the enlargement of Fig. 5 (bottom panel). From the inserted figure the Lyα absorption feature is apparent and is consistent with the neutral hydrogen column density of $8 \pm 2 \times 10^{20}$ cm^{-2} inferred from the spin pulsed spectrum. Hence, while this absorption in the orbital pulsation spectrum is clearly circumstellar, the same nature in the spin pulsed spectrum cannot be excluded.

The UV FOS spectrum requires a hot component with a blackbody temperature of 21 500±500 K (Fig. 5 bottom panel enlargement). The composite UV and optical broad band energy distrubution confirms the previous results on the presence of two

components, a hot at 19 500 $\pm$ 500 K and a cool one at 5 700 $\pm$ 200 K ($\chi^2_{\rm red} = 1.1$) (Fig. 5, bottom panel). With current UV observations, it is now possible to constrain the temperature of the hot emitting region. The temperature of the cool component is in agreement, within errors, with that inferred in Paper 1. A substantial increase by a factor of ~ 2.6 in the area of the hot region is found when compared to the 1990 epoch, which is $\sim 12\,{\rm A_{wd}}$. The emitting area of the cool component is instead similar to that previously derived (Paper 1).

8. Discussion

The HST/FOS and IUE spectroscopy has revealed new insights in the UV variability of FO Aqr.

8.1. The periodic variations

The UV continuum and emission line fluxes are found to be strongly variable at the orbital period. This periodicity also dominates the optical range where FO Aqr was previously found to be spin dominated. The time series analysis indicates the presence of other periodicities, the negative $\omega - 2\,\Omega$ sideband being much stronger than the beat $\omega - \Omega$ in both UV and optical ranges. The presence of sidebands with different amplitudes at different epochs is rather common in FO Aqr, although the beat is usually the strongest (Patterson & Steiner 1983; Warner 1986; Semeniuk & Kaluzny 1988, Chiappetti et al. 1989; Paper 1, Marsh & Duck 1996). In particular the intermittent occurrence of a stronger pulsation at $\omega - 2\,\Omega$ frequency was already noticed (Warner 1986; Patterson et al. 1998). The strong negative sideband $\omega - 2\,\Omega$, cannot be produced by an amplitude modulation at 2Ω frequency of the rotational pulses, since the positive sideband $\omega + 2\,\Omega$ should have been present. Also, an orbital variability of the amplitude of the $\omega - \Omega$ modulation cannot be responsible alone since it is too weak. Hence the $\omega - 2\Omega$ pulsation should be dominated by the effects of an unmodulated illumination from the white dwarf, which naturally gives rise to the orbital variability (Warner 1986).

The occurrence of coherence between spin and beat pulsations appears to be different from epoch to epoch (Semeniuk & Kaluzny 1988; Osborne & Mukai 1989; Paper 1). It was proposed that phase coherence close to the optical orbital minimum could be possible if the reprocessing site(s) are viewing the lower accreting pole (Paper 1). The observed shift of half an orbital cycle would then imply that the reprocessing region(s), are now viewing the main accreting pole, as predicted by the standard reprocessing scenario (Warner 1986).

The behaviour of UV emission lines is different between fluxes and V/R ratios. The line fluxes are strongly variable at the orbital period, the spin variability being 1.6 times lower. On the other hand, their V/R ratios only show a rotational S-wave, but that of C IV line is surprisingly weak. The lack of detection of an orbital S-wave, can be ascribed to the low amplitude ($\sim$ 300–400 $\rm km\,s^{-1}$) velocity displacements known from optical data (Hellier et al. 1989; Marsh & Duck 1996), which are not detected because of the low spectral resolution of the FOS data.

8.2. The rotational pulses

Both shapes and amplitudes of UV and optical continnum spin pulses indicate the presence of two components, one dominating the near-UV and optical ranges, already identified in Paper 1 and a new contribution dominating the far-UV pulses which lags by ~ 0.2 in phase the first one. Furthermore a different behaviour between emission line fluxes and V/R ratios is observed. While the latter show a spin S-wave in phase with the far-UV continuum, the line fluxes follow the near-UV and optical pulsations. The maximum blue-shift found at rotational maximum of the far-UV pulses indicates that the bulk of velocity motions in the emission lines maps the innermost regions of the accretion curtain. The outer curtain regions are then responsible for X-ray illumination effects seen in the line fluxes and near-UV and optical continua. A direct comparison with previous X-ray observations reported by Beardmore et al. (1998) is not possible since, adopting their linear spin ephemeris, the UV and optical maxima lag by $\Delta\Phi_{\rm spin}$=0.4 their predicted optical maximum. However, the X-ray pulse maxima observed by Beardmore et al. (1998), typically lag by $\Delta\Phi_{\rm spin}$ =0.2 their optical phase zero (see their Fig. 3), consistently with the lag observed between the far-UV and optical pulses. Hence this difference is an indication that the far sides of the accretion curtain come into view earlier than the innermost regions.

The spectrum of the pulsation reveals regions at $\sim$ 37 000 K covering a relatively large area, $\sim 0.1\,{\rm A_{wd}}$, with respect to typical X-ray fractional areas $f < 10^{-3}$ (Rosen 1992). Such hot components have been also observed in the IPs PQ Gem (Stavroyiannopoulos et al. 1997) and EX Hya (de Martino 1998). The presence of the ${\rm Ly}\alpha$ absorption feature in this spectrum can be partially due to the photospheric absorption of the heated white dwarf with similar temperature and fractional area as a blackbody representation. On the other hand, both orbital and rotational modulated spectra give similar values of $N_{\rm H}$ if this absorption is of circumstellar nature. Hence, while only in AE Aqr the UV pulses are clearly associated with the heated white dwarf (Eracleous & Horne 1994, 1996), those in FO Aqr can be associated with either the innermost regions of the accretion curtain onto the white dwarf or its heated polar regions.

The second component identified as a cool 12 000 K region covers $\sim 11{\rm A_{wd}}$, a factor ~ 1.5 lower than previously found in Paper 1. Thus the decrease in the optical amplitudes does not involve substantial changes in temperatures but in the size of the accretion curtain. Such lower temperatures characterizing the near-UV and optical pulses are also recognized in other IPs (de Martino et al. 1995; Welsh & Martell 1996; Stavroyiannopoulos et al. 1997; de Martino 1998). Although a two component pulsed emission might be a crude representation, it is clear that temperature gradients are present within the accretion curtain extending up to $\sim 6{\rm R_{wd}}$.

The bolometric flux involved in the spin modulation due to both components amounts to $6.3\times10^{-11}\,{\rm ergs\,cm^{-2}s^{-1}}$. Although no contemporary X-ray observations are available this accounts for $\sim 26\%$ the total accretion luminosity as derived from ASCA 1993 observations (Mukai et al. 1994).

8.3. The sidebands variability

The UV continuum pulsations observed at the sideband frequencies, $\omega - 2\Omega$, $\omega - \Omega$ and $\omega + \Omega$, indicate the presence of a relatively hot component $\sim$ 20 000–25 000 K. The lack of adequate data in the optical range does not allow one to confirm the cool ($\sim$ 7 000 K), and hence possible second component, in the beat pulsed energy distribution as found in Paper 1. The phase lags of the far-UV maximum with respect to that in the near-UV in the $\omega - \Omega$ and $\omega + \Omega$ pulsations are similar to that observed in the rotational pulses. This is consistent with the pulsations being produced by amplitude variations of the spin pulses at the orbital period. In contrast, the prominent negative sideband $\omega - 2\Omega$ variability is not affected by phase shift effects, indicating that indeed such variability is mainly due to an aspect dependence of the reprocessing site at the orbital period.

No strong pulsation in the UV emission lines is observed at these frequencies except for the interesting anti-phased behaviour of these lines at the beat period. These are observed as weak absorption features in the modulated spectrum. Such behaviour, although much more prominent, is also observed in the IP PQ Gem (Stavroyiannopoulos et al. 1997). Though this is not easy to understand, a possibility could be that the reprocessing site, producing the $\omega - \Omega$ component in the emission lines, is viewing the lower pole instead of the main X-ray illuminating pole as also suggested by Stavroyiannopoulos et al. (1997).

8.4. The orbital variability

The present study confirms previous results where the orbital modulation is composed by two contributions, identified as the illuminated bulge and the heated face of the secondary star, the former being at superior conjunction at $\Phi_{\rm orb}$ = 0.86, while the latter is at superior conjunction at $\Phi_{\rm orb}$ = 0.0. The double-humped maximum in the optical light curve can be understood in terms of relative proportion of a strong bulge contribution with respect to that of the secondary star. Indeed no changes in the temperatures are found (the hot one is better constrained with the present data), but a substantial change by a factor of $\sim$ 2.6 since 1990 is found in the emitting area of the bulge itself. All this indicates that illumination effects are basically unchanged whilst the inflated part of the disc has increased.

The total bolometric flux involved in the orbital variability amounts to $2.7\times10^{-10}\,\mathrm{ergs\ cm^{-2}s^{-1}}$which is a factor ~ 4 larger than that of the rotational pulsation. Neglecting the sideband contributions at first approximation, the total modulated flux amounts to $3.3\times10^{-10}\,\mathrm{ergs\ cm^{-2}s^{-1}}$and corresponds to a reprocessed luminosity of $4.2 \times 10^{33}\,\mathrm{ergs\ s^{-1}}$which is approximately the order of magnitude of the accretion luminosity derived from X-rays (Mukai et al. 1994). Then assuming the balance of the energy budgets of the reprocessed and primary X-ray radiations, and hence of the accretion luminosity, an estimate of the accretion rate of $\dot{\rm M} = 6.7 \times 10^{-10}\,{\rm M}_\odot\,{\rm yr}^{-1}$ is derived.

8.5. The long term variability

FO Aqr has displayed a change in its power spectrum at optical and UV wavelengths on a time scale of five years. It was also brighter by 0.3 mag and 0.2 mag in the two ranges with respect to 1990. This difference is accounted for by the orbital modulated flux. The study of the spectra of the periodic variabilities has shown that a shrinking of the accretion curtain by a factor of $\sim$ 1.5 has occurred while the inflated part of the disc has increased in area by a factor of 2.6. Such changes indicate variations in the accretion parameters. Worth noticing is that the unmodulated UV and optical continuum component has not changed with time, indicating that the steady emission from the accretion disc (Paper 1) has not been affected. These results are in agreement with the long term trend of the X-ray power spectra (Beardmore et al. 1998) which showed that FO Aqr was dominated by the spin pulsation in 1990, while in 1988 and in 1993 prominent orbital and sideband variabilities were present. Changes from a predominant disc-fed accretion to a disc-overflow (or stream-fed) accretion have been the natural explanation for such changes in the X-ray power spectra. As proposed in Paper 1, the bulge provides a source for a variable mass transfer onto the white dwarf, and an increase in its dimensions accounts for a predominant disc-overflow towards the white dwarf.

Beardmore et al. (1998) suggested that changes in the accretion mode could be triggered by variations in the mass accretion rate and the analysis presented here is indeed in favour of this hypothesis. An estimate of changes in the accretion rate producing a shrinking of the accretion curtain can be inferred by the relation betwen magnetospheric radius, accretion rate and magnetic moment (Norton & Watson 1989):

$$r_{mag} = \phi\, 2.7 \times 10^{10}\, \mu_{33}^{4/7}\, \dot{M}_{16}^{-2/7}\, M_{wd}^{-1/7} \qquad (2)$$

where $\phi \lesssim 1$ is a dimensionless factor accounting for a departure from spherical symmetry, μ_{33} is the magnetic moment in units of $10^{33}\,\mathrm{G\,cm^3}$, $\dot{\rm M}_{16}$ is the mass accretion rate in units of $10^{16}\,\mathrm{g\,s^{-1}}$ and $\rm M_{wd}$ is the white dwarf mass in units of $\rm M_\odot$. Hence assuming that the accretion curtain reaches the magnetospheric boundary, a reduction of the linear extension by a factor of $\sim$ 1.2 implies that the accretion rate has increased by a factor $\sim$ 2 in five years.

The long term spin period variations observed from 1981 to 1997 in FO Aqr (Patterson et al. 1998), which changed from a spin-down to a recent spin-up since 1992, were proposed to be due to variations around the equilibrium period produced by long term variations in $\dot{\rm M}$. The increase in brightness level and the results found in the present analysis are strongly in favour of this interpretation.

9. Conclusions

The present HST/FOS and IUE spectroscopy has allowed us for the first time to infer the characteristics of multiple periodicities in the UV emission of FO Aqr. Also, coordinated optical photometry has provided further constraints summarized as follows:

1) The rotational pulsations in the UV and optical are consistent with the current accretion curtain scenario. They reveal the presence of strong temperature gradients within the curtain moving from the footprints onto the white dwarf surface to several white dwarf radii. A spin S-wave is observed in the UV emission lines which maps the innermost regions of the accretion curtain.
2) Orbital sideband variabilities indicate that reprocessing is occurring at fixed regions within the binary frame. Different behaviour is observed in the emission lines and continuum beat pulses indicating a complex reprocessing scenario.
3) The orbital UV variability is confirmed to arise from the illuminated side of the inflated disc (bulge) while the optical modulation is produced by heating effects at the secondary star.
4) A change in the relative proportion of rotational and orbital modulation amplitudes is found on a timescale of five years. These are interpreted as a reduction in the dimensions of the accretion curtain accompained by an increase in the bulge size.

These observations indicate a long term change in the accretion mode where FO Aqr has switched from a disc-fed to a disk-overflow state triggered by changes in the mass accretion rate.

Acknowledgements. The authors wish to acknowledge the valuable help from ST ScI staff who provided new calibration files for the square apertures of FOS instrument before publication. J. Patterson is gratefully acknowledged for providing the new revised spin ephemeris quoted in the text.

References

Beardmore A.P., Mukai K., Norton A.J., et al., 1998, MNRAS 297, 337
Bohlin R.C., 1975, ApJ 200, 402
Buckley D.A.H., 1996, In: Evans A., Wood J.H. (eds.) Proc. Cataclysmic Variables and Related Objects. IAU Coll. 158, Space Sci. Lib. 208, p. 185
Chiappetti L., Bonnet-Bidaud J.-M., Del Gratta C., et al., 1989, ApJ 342, 493
Deeming T.J., 1975, Ap&SS 36, 137
de Martino D., 1993, In: Regev O., Shaviv G. (eds.) Proc. 2nd Haifa Conference on: Cataclysmic Variables and related physics. p. 201
de Martino D., 1995, In: Buckley D.A.H., Warner B. (eds.) ASP Conf. Ser. 85, Cape Workshop on Magnetic Cataclysmic Variables. p. 238
de Martino D., 1998, In: Gonzalez-Riestra R., Wamsteker W., Harris R. (eds.) ESA SP-413, Ultraviolet Astrophysics Beyond the IUE Final Archive. p. 387
de Martino D., Buckley D.A.H., Mouchet M., Mukai K., 1994, A&A 284, 125 (Paper 1)
de Martino D., Mouchet M., Bonnet-Bidaud J.M., et al., 1995, A&A 298, 849
Dickey J.M., Lockman G.J., 1990, ARA&A 28, 215
Eracleous M., Horne K., 1994, ApJ 433, 313
Eracleous M., Horne K., 1996, ApJ 471, 427
Garhart M.P., Smith M.A., Levay K.L., et al., 1997, International Ultraviolet Explorer New SPectral Image Processing Information Manual. Version 2.0
Gonzalez-Riestra R., 1998, In: Gonzalez-Riestra R., Wamsteker W., Harris R. (eds.) ESA SP-413, UV Astrophysics beyon the IUE Final Archive. p. 707
Hellier C., 1993, MNRAS 265, L5
Hellier C., 1995, In: Buckley D.A.H., Warner B. (eds.) ASP Conf. Ser. 85, Cape Workshop on Magnetic Cataclysmic Variables. p. 185
Hellier C., Mason K., Cropper M., 1989, MNRAS 237, 39P
Hellier C., Mason K., Cropper M., 1990, MNRAS 242, 250
Marsh T.R., Duck S.R., 1996, New Astron. 1, 97
Mauche C.W., Lee Y.P., Kallman T.R., 1997, ApJ 477, 832
Mukai K., Ishida M., Osborne J.P., 1994, PASJ 48, L87
Norton A.J., Watson M.G., 1989, MNRAS 237, 715
Norton A.J., Hellier C., Beardmore A.P., et al., 1997, MNRAS 289, 362
Osborne J.P., Mukai K., 1989, MNRAS 238, 1233
Patterson J., 1994, PASP 106, 209
Patterson J., Steiner J.E., 1983, ApJ 264, L61
Patterson J., Kemp J., Richman H.R., et al., 1998, PASP 110, 415
Roberts D.H., Lehár J., Dreher J.W., 1987, AJ 93, 968
Rosen S.R., 1992, MNRAS 254, 493
Rosen S.R., Mason K.O., Cordova F.A, 1988, MNRAS 231, 549
Semeniuk I., Kaluzny J., 1988, Acta Astron. 38, 49
Shull J.M., van Steenberg M.E., 1985, ApJ 298, 268
Silber A.D., Anderson A.F., Margon B., et al. 1996, ApJ 462, 428
Stavroyiannopoulos D., Rosen S.R., Watson M.G., et al., 1997, MNRAS 288, 891
Warner B., 1986, MNRAS 219, 347
Warner B., 1995, Cataclysmic Variable Stars. Cambridge Univ. Press, Cambridge
Welsh W.F, Martell P.J., 1996, MNRAS 282, 739